NASA Contractor Report 172561

ICASE REPORT NO. 85-19

NASA-CR-172561
19850013265

ICASE

A THREE-DIMENSIONAL SPECTRAL ALGORITHM FOR SIMULATIONS OF TRANSITION AND TURBULENCE

Thomas A. Zang

M. Yousuff Hussaini

INSTITUTE FOR COMPUTER APPLICATIONS IN SCIENCE AND ENGINEERING
NASA Langley Research Center, Hampton, Virginia 23665

Operated by the Universities Space Research Association

National Aeronautics and
Space Administration

Langley Research Center
Hampton, Virginia 23665

A THREE-DIMENSIONAL SPECTRAL ALGORITHM FOR SIMULATIONS OF TRANSITION AND TURBULENCE

Thomas A. Zang
NASA Langley Research Center

and

M. Yousuff Hussaini
Institute for Computer Applications in Science and Engineering

Abstract

A spectral algorithm for simulating three-dimensional, incompressible, parallel shear flows is described. It applies to the channel, to the parallel boundary layer, and to other shear flows with one wall-bounded and two periodic directions. Representative applications to the channel and to the heated boundary layer are presented.

Research was supported by the National Aeronautics and Space Administration under NASA Contract NAS1-17070 while the second author was in residence at ICASE, NASA Langley Research Center, Hampton, VA 23665.

Nomenclature

$\hat{i}$	unit vector in x-direction
k	normal wavenumber in model problem
p	pressure
t	time
u	streamwise velocity
v	normal velocity
w	spanwise velocity
x	streamwise coordinate
y	normal coordinate
z	spanwise coordinate
k_x	scaled streamwise wavenumber
k_z	scaled spanwise wavenumber
m_p	pressure gradient exponent
$\hat{u}_{k_x,k_z}$	velocity after transforms in x and z
$\tilde{u}_{k_x,m,k_z}$	velocity after transforms in x, y, and z
C_p	specific heat
F	velocity function in Falkner-Skan equations
F_w	suction parameter
H	temperature function in Falkner-Skan equations
I	identity matrix
N_x	number of grid points in x
N_y	number of grid points in y
N_z	number of grid points in z
Re	Reynolds number

T	temperature
T_m	Chebyshev polynomial of degree m
T_w	wall temperature
α	streamwise wavenumber
β	spanwise wavenumber
β_p	pressure gradient parameter
$\delta_{k,\ell}$	Kronecker delta function
δ^*	displacement thickness
κ	conductivity
η	boundary layer similarity variable
σ	Prandtl number
ρ	density
ν	kinematic viscosity
θ	scaled temperature
τ	heating parameter
ω	temporal frequency
Δt	time-step
Δy	grid spacing in normal direction

subscripts

k	component for normal wavenumber k
e	right-hand side of linear equations
∞	free stream values
0	equilibrium values
ℓ	iteration parameter

INTRODUCTION

The development of accurate and efficient spectral methods has made feasible the reliable, three-dimensional simulation of the early stages of transition in parallel shear flows. Orszag and Kells[1] pioneered the numerical work on channel flow. They demonstrated that linearly stable two-dimensional Tollmein-Schlichting waves can exhibit a strong secondary instability to three-dimensional disturbances of the Benney-Lin[2] type for Reynolds numbers as low as 1000. Wray and Hussaini[3] presented compelling evidence for the use of the parallel flow approximation in their Blasius boundary-layer simulation. Their calculation reproduced the essential features of the Kovasznay, et al.[4] experiment up to the two-spike stage. The presence of strong secondary instabilities in several other linearly stable, parallel flows has been demonstrated by Orszag and Patera.[5] An extensive comparison of numerical simulation with the channel flow experiments of Nishioka, et al.[6] has been made by Kleiser and Schumann.[7]

The calculations cited above all employed algorithms which use direct methods for solving the implicit equations resulting at each time-step from the spatial discretization. The same is true for a recent novel spectral algorithm for curved channel flow.[8] The cost of these direct solution methods is increased substantially by the addition of even minor geometric terms or the temporal variation of the viscosity which is essential for assessing the more subtle effects of heating. This is a major consideration which has led us to develop an algorithm which resorts to iterative methods for the solution of the implicit equations.

This paper is devoted to a description of an algorithm for transition simulation which is based on iterative methods. It shares some common

features with a method developed by Morchoisne.[9] The description focuses on the controlled boundary-layer algorithm since this problem is more involved than the channel and has not yet been simulated numerically.

BASIC EQUATIONS FOR THE PARALLEL BOUNDARY LAYER

Mean Flow

We require the incompressible boundary-layer equations that include the effects of pressure gradient, suction, and/or heating. Viscous dissipation is neglected, and the pressure gradient and suction distributions are chosen compatible with similarity solutions. The Falkner-Skan equations[10] are

$$(\bar{\mu}F'')' + m_p(1 - F'^2) + \frac{1}{2}(m_p + 1)FF'' = 0, \tag{1}$$

$$(\bar{\kappa}H')' + \sigma\frac{1}{2}(m_p + 1)FH' = 0, \tag{2}$$

with the boundary conditions

$$\begin{aligned} F(0) &= F_w \\ F'(0) &= 0 \\ F'(\infty) &= 1 \\ H(0) &= 1 \\ H(\infty) &= 0. \end{aligned} \tag{3}$$

A prime denotes differentiation with respect to the similarity variable

$$\eta = y\sqrt{u_\infty/\nu_\infty x} \ .$$

The free-stream velocity u_∞ is proportional to x^{m_p}.

The fluid properties are scaled with respect to their free-stream values (with $\bar{\rho}_\infty = 1$):

$$\bar{\mu} = \mu(T)/\mu_\infty$$

$$\bar{\kappa} = \kappa(T)/\kappa_\infty$$

$$\sigma = \mu_\infty C_p(T_\infty)/\kappa_\infty .$$

The dimensional velocities and temperatures are related to the similarity variables via

$$u = u_\infty F(\eta)$$

$$v = \frac{1}{2}\sqrt{\frac{\nu_\infty u_\infty}{x}}\left[\eta F'(\eta) - (m_p+1)F(\eta)\right]$$

$$T = (T_w - T_\infty)H(\eta) + T_\infty .$$

The parameter m_p is related to the conventional pressure gradient parameter β_p by

$$m_p = \frac{\beta_p}{2 - \beta_p} \ .$$

The wall suction is controlled by F_w and the heating effects by T_∞ and T_w. The Reynolds number is based on free-stream velocity, viscosity, and the

displacement thickness δ^* of the uncontrolled boundary layer:

$$\delta^* = 1.72 \sqrt{\frac{u_\infty x}{\nu_\infty}} .$$

The results in this paper pertain to water boundary layers, for which the appropriate empirical formulas[11] are

$$\mu(T) = 1.002\ e^{r(T)}$$

$$r(T) = -2.303\ \left|1.370 + 8.36 \times 10^{-4}(T-293)\right|(T-293)/(T-164)$$

$$\kappa(T) = -9.901 + 0.1002\ T - 1.874 \times 10^{-4}T^2 + 1.040 \times 10^{-7}T^3$$

$$C_p(T) = 41.84 \times \left[2.140 - 9.68 \times 10^{-3}T + 2.69 \times 10^{-5}T^2 - 2.42 \times 10^{-8}T^3\right]. \quad (4)$$

All the results below are for a free-stream temperature $T_\infty = 293^0$K.

The numerical solutions of equations (1)-(3) were obtained by a fourth-order compact finite difference scheme,[12] with a typical accuracy of 7 significant digits.

As noted in the introduction, the parallel flow assumption has been used in this work: having fixed a reference location x in the streamwise direction we presume that the streamwise velocity u(y) and the temperature T(y) are the same at all x and that the normal velocity v(y) is zero. This "mean flow" is not a solution to the Navier-Stokes equations. For consistency, then, we imagine that the Navier-Stokes equations also include a small forcing term so

that the "mean flow" is an equilibrium solution to the full nonlinear equations.

In the remainder of this paper, the fluid equations will be used in dimensionless form, and the overbars on $\overline{\mu}$ and $\overline{\kappa}$ will be dropped. Velocities are scaled by u_∞, lengths by δ^*, and densities by ρ_∞. The temperature variable θ is, as usual,

$$\theta = \frac{T - T_\infty}{T_w - T_\infty} .$$

The parameters which define a particular case, then, are the Reynolds number Re, the pressure gradient parameter β_p, the suction parameter F_w, and the heating parameter $\tau = T_w/T_\infty$.

Linearized Equations

Initial conditions for the numerical simulations are based on solutions to the Orr-Sommerfeld and Squire equations for small amplitude velocity perturbations. Temperature fluctuations have been ignored in these linearized equations, but the effect of the mean temperature upon the viscosity and mean flow profiles is included. Velocity perturbations are taken to be of the form

$$u(x,y,z,t) = \hat{u}(y)e^{i(\alpha x + \beta z - \omega t)}$$

for real α and β. The Orr-Sommerfeld and Squire eigenvalue problems are solved by a Chebyshev tau method.[13] The Chebyshev expansions are in terms of the computational variable ξ, which is related to the physical variable y by the algebraic mapping

$$y = y_e \frac{1 + \xi}{1 + \frac{2y_e}{y_{max}} - \xi} . \tag{5}$$

The parameter y_e is roughly twice the normal distance at which u = 0.5, and y_{max} is the upper boundary in the physical domain. A typical choice for y_{max} is 15, which is roughly 5 times the boundary-layer thickness. The variable ξ has the usual Chebyshev distribution in [-1,1]:

$$\xi_i = \cos \frac{\pi i}{N_y} , \qquad i=0,1,\ldots,N_y .$$

Roughly half the points fall within the displacement thickness, and two-thirds are within the boundary-layer thickness.

Between 50 and 70 Chebyshev polynomials are used for the solution of the linear eigenvalue problems. The major source of error is inaccuracies in the numerical solution of the mean flow. Nonetheless, the eigenvalues and eigenfunctions are reliable to 5 or 6 digits.

Navier-Stokes Equations

The nonlinear simulations are performed for the equations

$$\underline{u}_t + \underline{\omega} \times \underline{u} = -\nabla P + \nabla \cdot (\mu \nabla \underline{u}) + f\hat{i} \tag{6}$$

$$\theta_t + \underline{u} \cdot \nabla\theta = \nabla \cdot (\kappa \nabla\theta) + g \tag{7}$$

$$\nabla \cdot \underline{u} = 0 \tag{8}$$

where the vorticity $\underline{\omega} = \nabla \times \underline{u}$, the total pressure $P = p + \frac{1}{2} |\underline{u}|^2$, and the boundary conditions are

$$\begin{matrix} \underline{u} = 0 \\ \theta = 0 \end{matrix} \quad \text{at} \quad y = 0, \qquad \begin{matrix} \underline{u} = 1 \\ \theta = 1 \end{matrix} \quad \text{at} \quad y = \infty. \tag{9}$$

The forcing functions are given in terms of the mean flow variables by

$$\begin{aligned} f &= -\frac{\partial}{\partial y}\left(\mu_0 \frac{\partial u_0}{\partial y}\right) \\ g &= -\frac{\partial}{\partial y}\left(\kappa_0 \frac{\partial \theta_0}{\partial y}\right). \end{aligned} \tag{10}$$

They ensure that the mean flow is a stationary solution of Equations (6) - (8).

NUMERICAL METHOD

Discrete Equations

The nonlinear three-dimensional calculations reported below are based on the algorithm described for two-dimensional flow in Reference 14. The spatial discretization is Fourier-collocation in x and z and Chebyshev collocation in y. The temporal discretization is backward Euler for the pressure, Crank-Nicolson for the normal diffusion and conduction terms, and third- or fourth-order Adams-Bashforth for the remaining terms in Equations (6) and (7). The continuity equation is enforced as a constraint at the new time level.

The primitive variables have two series representations which will be useful in this discussion. The first is

$$u(x,y,z,t) = \sum_{k_x = -N_x/2}^{\frac{N_x}{2} - 1} \sum_{k_z = -N_z/2}^{\frac{N_z}{2} - 1} \hat{u}_{k_x,k_z}(y,t) e^{i(\hat{k}_x x + \hat{k}_z z)} \tag{11}$$

where $\hat{k}_x = \frac{2\pi}{L_x} k_x$, $\hat{k}_z = \frac{2\pi}{L_z} k_z$, and L_x and L_z are the lengths of the (periodic) domain in the x and z directions, respectively. The second involves the additional series

$$\hat{u}_{k_x,k_z}(y,t) = \sum_{m=0}^{N_y} \tilde{u}_{k_x,m,k_z}(t)\, T_m(\xi), \tag{12}$$

where ξ is related to y by Equation (5). Henceforth, the subscripts k_x, m, and k_z will not be written explicitly unless necessary. The collocation points in the periodic directions are

$$\begin{aligned} x_i &= \frac{2\pi i}{N_x L_x}, & i &= 0,1,\ldots,N_x-1 \\ z_k &= \frac{2\pi k}{N_z L_z}, & k &= 0,1,\ldots,N_z-1. \end{aligned} \tag{13}$$

A staggered grid is employed in the normal direction. Velocities and temperatures are defined at the points

$$\xi_j = \cos\frac{\pi j}{N_y}, \qquad j = 0,1,\ldots,N_y \tag{14}$$

and the pressures at

$$\xi_{j+1/2} = \cos\frac{\pi(j+1/2)}{N_y}, \quad j = 0,1,\ldots,N_y-1. \tag{15}$$

The continuity equation is enforced at the latter points and the remaining equations at the former ones. The staggered grid avoids artificial pressure boundary conditions, precludes spurious pressure modes, and facilitates the solution of the algebraic equations which arise from the implicit terms in the time discretization.

Chebyshev interpolation is the natural process for transferring variables between the grids of Equations (14) and (15). For example, consider the velocity component u. Let u_j, for $j = 0,1,\ldots,N_y$, denote its values at the points (14). The Chebyshev coefficients are given by the usual quadrature rule

$$\tilde{u}_m = \frac{2}{N_y \bar{c}_m} \sum_{j=0}^{N_y} \bar{c}_j^{-1} u_j \, T_m(\xi_j) = \frac{2}{N_y \bar{c}_m} \sum_{j=0}^{N_y} \bar{c}_j^{-1} u_j \cos\frac{m\pi j}{N_y}, \quad m = 0,1,\ldots,N_y \tag{16}$$

where

$$\bar{c}_m = \begin{cases} 2 & m = 0 \text{ or } N_y \\ 1 & 1 \leq m < N_y . \end{cases}$$

The interpolated values of u are

$$u_{j+1/2} = \sum_{m=0}^{N_y-1} \tilde{u}_m \, T_m(\xi_{j+1/2}) = \sum_{m=0}^{N_y-1} \tilde{u}_m \cos\frac{(j+1/2)\pi m}{N_y}, \quad j = 0,1,\ldots,N_y-1. \tag{17}$$

[Note that $T_{N_y}(\xi_{j+1/2}) = 0$ for $j=0,1,\ldots,N_y-1$.] The Fast Fourier Transform (FFT) may be used to evaluate both sums (16) and (17). The less familiar sum in Equation (17) over the odd cosines may be handled by the technique presented in Appendix C of Reference 15.

The temporal discretization of Equations (6)-(8) leads, after a Fourier transform in x and z, to an implicit system of the form

$$\hat{u}^{n+1} - (b\hat{u}_y^{n+1})_y + i\hat{k}_x\gamma\hat{q}^{n+1} = \hat{u}_e$$

$$\hat{v}^{n+1} - (b\hat{v}_y^{n+1})_y + \gamma\hat{q}_y^{n+1} = \hat{v}_e \qquad \text{at } \xi_j$$

$$\hat{w}^{n+1} - (b\hat{w}_y^{n+1})_y + i\hat{k}_z\gamma\hat{q}^{n+1} = \hat{w}_e \tag{18}$$

$$-i\hat{k}_x\,\gamma^*\,\hat{u}^{n+1} - \gamma^*\hat{v}_y^{n+1} - i\hat{k}_z\gamma^*\hat{w}^{n+1} = 0 \quad \text{at } \xi_{j+1/2} \tag{19}$$

along with Dirichlet boundary conditions on the velocities. An * denotes the complex conjugate. The coefficient $b = \frac{1}{2}\,\Delta t\,\mu^n_{avg}(y,t)$, where the last term is the average value of $\mu^n(x,y,z,t)$ at fixed y and t. The pressure has been included in terms of the scaled variable $\hat{q} = (\frac{\Delta t}{\gamma})\hat{P}$, where γ is a complex constant whose role is explained below. Similarly, the temperature equation is

$$\hat{\theta}^{n+1} - (d\hat{\theta}_y^{n+1})_y = \hat{\theta}_e \qquad \text{at } \xi_j \tag{20}$$

subject to Dirichlet boundary conditions, where $d = \frac{1}{2}\,\Delta t\,\kappa^n_{avg}(y,t)$. The right-hand-sides of these equations contain the explicit terms in the temporal

discretization. Let

$$U = (\hat{u}_0^{n+1}, \hat{u}_1^{n+1}, \ldots, \hat{u}_{N_y}^{n+1}),$$

$$Q = (\hat{q}_{1/2}^{n+1}, \hat{q}_{3/2}^{n+1}, \ldots, \hat{q}_{N_y-1/2}^{n+1})$$

and define V, W, and Θ similarly to U. Let D_b and D_d be diagonal matrices with the elements of b and d on their respective diagonals. Let the effect of Equations (16) and (17) on U be denoted by A_+ and the reverse interpolation procedure (for Q) by A_0. Finally, let M denote the matrix which represents Chebyshev differentiation in the y direction. Then Equations (18) to (20) reduce to the algebraic set

$$\begin{aligned}
(I - MD_bM)U + i\hat{k}_x\gamma A_0 Q &= U_e \\
(I - MD_bM)V + \gamma M A_0 Q &= V_e \\
(I - MD_bM)W + i\hat{k}_z\gamma A_0 Q &= W_e,
\end{aligned} \tag{21}$$

$$-i\hat{k}_x\gamma^* A_+ U - \gamma^* A_+ MV - i\hat{k}_z\gamma^* A_+ W = 0 \tag{22}$$

$$(I - MD_dM)\Theta = \Theta_e \tag{23}$$

where the first and last rows of (21) and (23) are replaced by the boundary conditions. Clearly, the equations for each pair $(\hat{k}_x, \hat{k}_z)$ are independent. Moreover, Equation (23) is not coupled to Equations (21) and (22) and thus may be solved separately. The matrices A_0, A_+, and M are full. Except in special cases the direct solution of these equations is not practical.

The iterative solution of Equation (23) is straightforward: simply precondition the system by a finite-difference approximation on the Chebyshev grid[16] and apply a standard iterative method[17] such as Richardson,[16] Chebyshev acceleration,[16] minimum residual,[18] or even multigrid.[19] The finite-difference system is tridiagonal and positive definite.

The key to this algorithm is the solution of the system (21)-(22). A simplified model problem, discussed in the following sub-section, is instructive.

Model Problem Discussion

Suppose that the boundary conditions in the normal direction are periodic instead of Dirichlet and that the viscosity, i.e., b, is constant. Replace the Chebyshev discretization with a Fourier one, on, say $[0,2\pi]$. Then the vertical collocation points are

$$y_j = \frac{2\pi j}{N_y} \qquad j=0,1,\ldots,N_y-1$$

$$y_{j+1/2} = \frac{2\pi(j+1/2)}{N_y} \qquad j=0,1,\ldots,N_y-1.$$

The fully discrete equations may be cast in a form analogous to (21)-(22), where now

$$\begin{aligned} M &= C_0^* D C_0 \\ MD_b M &= bC_0^* D^2 C_0 \\ A_0 &= C_0^* C_+ \end{aligned} \tag{24}$$

$$A_+ = C_+^* C_0$$

and

$$(C_0)_{k,j} = \frac{1}{\sqrt{N_y}} e^{-iky_j}, \qquad j= 0,1,\ldots,N_y-1$$
$$k= -N_y/2,\ -N_y/2+1,\ldots,N_y/2-1$$

$$(C_+)_{k,j} = \frac{1}{\sqrt{N_y}} e^{iky_{j+1/2}},$$

$$D_{k,\ell} = ik\delta_{k,\ell}, \qquad k,\ell = -N_y/2,\ -N_y/2+1,\ldots,N_y/2-1.$$

Thus, we have for the spectral equations

$$\begin{aligned}
(I - bC_0^*\ D^2\ C_0)U + i\hat{k}_x\ \gamma C_0^*\ C_+\ Q &= U_e \\
(I - bC_0^*\ D^2\ C_0)V + \gamma C_0^*\ DC_+\ Q &= V_e \qquad (25) \\
(I - bC_0^*\ D^2 C_0)W + i\hat{k}_z\ \gamma C_0^*\ C_+\ Q &= W_e
\end{aligned}$$

$$-i\hat{k}_x\ \gamma^* C_+^*\ C_0\ U - \gamma^* C_+^*\ D^* C_0\ V - i\hat{k}_z\ \gamma^* C_+^*\ C_0\ W = 0. \qquad (26)$$

This can be written as the system

$$LX = B \qquad (27)$$

where, for instance, $X = (U, V, W, Q)$. Now let $\tilde{U}_k = C_0\ U$, $\tilde{Q}_k = C_+\ Q$ $\tilde{X} = RX$, and $\tilde{L} = RLR^*$ where

$$R = \begin{pmatrix} C_0 & 0 & 0 & 0 \\ 0 & C_0 & 0 & 0 \\ 0 & 0 & C_0 & 0 \\ 0 & 0 & 0 & C_+ \end{pmatrix}.$$

After a permutation of the rows and columns of $\tilde{L}$, we obtain a block diagonal matrix with blocks

$$\tilde{L}_k \, \tilde{X}_k = \tilde{B}_k \tag{28}$$

$$\tilde{X}_k = (\tilde{u}_k, \tilde{v}_k, \tilde{w}_k, \tilde{q}_k),$$

$$\tilde{L}_k = \begin{pmatrix} 1+bk^2 & 0 & 0 & i\hat{k}_x\gamma \\ 0 & 1+bk^2 & 0 & ik\gamma \\ 0 & 0 & 1+bk^2 & i\hat{k}_z\gamma \\ -i\hat{k}_x\gamma^* & -ik\gamma^* & -i\hat{k}_z\gamma^* & 0 \end{pmatrix}. \tag{29}$$

Consider now a finite-difference approximation to this model problem. Let E denote the foward shift operator subject to periodic boundary conditions. Then Equations (21)-(22) become

$$\left[I - \frac{b}{(\Delta y)^2}(E - 2I + E^{-1})\right]U + i\hat{k}_x\gamma \frac{1}{2}(E + I)Q = U_e$$

$$\left[I - \frac{b}{(\Delta y)^2}(E - 2I + E^{-1})\right]V + \frac{\gamma}{\Delta y}(E - I)Q = V_e \tag{30}$$

$$\left[I - \frac{b}{(\Delta y)^2}(E - 2I + E^{-1})\right]W + i\hat{k}_z\gamma \frac{1}{2}(E + I)Q = W_e,$$

$$- i\hat{k}_x\gamma^* \frac{1}{2}(I + E^{-1})U - \frac{\gamma^*}{\Delta y}(I - E^{-1})V - i\hat{k}_z\gamma^* \frac{1}{2}(I + E^{-1})W = 0. \tag{31}$$

Denote the matrix which represents the left-hand-side by H. This system can be reduced to block-diagonal form by the same transformation that was used for the spectral operator. The result can be written

$$\tilde{H}_k \tilde{X}_k = \tilde{B}_k \tag{32}$$

$$\tilde{H}_k = \begin{pmatrix} 1+bk^2s^2 & 0 & 0 & i\hat{k}_x\gamma a \\ 0 & 1+bk^2s^2 & 0 & ik\gamma s \\ 0 & 0 & 1+bk^2s^2 & i\hat{k}_z\gamma a \\ -i\hat{k}_x\gamma^* a & -ik\gamma^* s & -i\hat{k}_z\gamma^* a & 0 \end{pmatrix} \tag{33}$$

where

$$s = \frac{\sin(k\Delta y/2)}{(k\Delta y/2)} , \tag{34}$$

$$a = \cos(\frac{k\Delta y}{2}) . \tag{35}$$

The relevant range is $|k\Delta y| \leq \pi$.

If a and s were identically one, then the preconditioning would be perfect. In any case, the derivative terms cause no serious problem for $(2/\pi) \leq s \leq 1$. It is the averaging operator a which is a source of potential difficulty. As $|k\Delta y| \to \pi$, the averaging becomes useless. We anticipate difficulty only in circumstances for which $\hat{k}_x$ and/or $\hat{k}_z$ are large relative to the reciprocal of the grid spacing in y.

A preconditioned Richardson iteration for Equation (27) reads

$$X \leftarrow X - \Omega H^{-1}(B - LX) \tag{36}$$

where Ω is an iteration parameter. The choice of Ω and indeed the convergence properties of this scheme depend upon the eigenvalues of $H^{-1}L$. A (complex) Chebyshev acceleration of the basic Richardson scheme can be devised provided that all the eigenvalues of $H^{-1}L$ have positive real parts.[20]

The eigenvalues of the model problem are especially easy to obtain: since H and L were block-diagonalized by the same transformation, we need only compute the eigenvalues of $\tilde{H}_k^{-1}\tilde{L}_k$ for $k=1,2,\ldots,N_y/2$. Some results are shown in Figure 1. In these calculations $\hat{k}_z$ has been set to zero. Similar calculations for both $\hat{k}_x$ and $\hat{k}_z$ non-zero lead to qualitatively similar results. Figure 1(a) portrays the easiest of these 6 cases for the iterative scheme. Most of the eigenvalues are near unity, and they are located near the real axis between 1 and $\pi/2$. The eigenvalue spread in part (b) for $\hat{k}_x = 30$ is much larger. Nevertheless, the real parts of the eigenvalues are safely greater than zero. A comparison of parts (b), (c), and (d) reveals that for fixed $\hat{k}_x$ the eigenvalue spread is reduced as the vertical resolution is increased. The heuristic explanation for this welcome behavior is that as N_y increases, the eigenvalues of the first derivative operator become more important than those of the averaging operator. In actual numerical simulations the number of points in the x and y directions is likely to be nearly the same. Part (d) corresponds to the worst case that would arise in a 64^3 calculation. Parts (e) and (f) show the eigenvalue spectrum for a situation in which the viscosity is quite considerable. The major difference from the previous cases is the presence of additional eigenvalues along the real axis as large as $\pi^2/4$. This is characteristic of preconditionings of second-derivative spectral operators.

Clearly, the major shortcoming of this particular preconditioning is its treatment of the averaging operator. If the 2/3 rule is used to de-alias the collocation approximation in the normal direction, then the averaging operator is well-behaved. In this event, $|k\Delta y| \leq 2\pi/3$, so that $1/2 \leq a \leq 1$. For the case shown in Figure 1(b), the largest 6 eigenvalues disappear. With the use of the 2/3 rule, this case becomes quite manageable.

In the next sub-section, we present numerical evidence that the model problem predicts very well the eigenvalues of the system of real interest. Already the model problem suggests that the major shortcoming of the preconditioning is its treatment of the averaging operator. Fortunately, the model problem provides a ready tool with which to check the effectiveness of alternative preconditionings.

A Minimum Residual Iterative Scheme

The actual system that must be solved is given by Equations (21) and (22). It clearly can be written in the form of Equation (27) by an obvious adaptation of the notation of the previous sub-section. Likewise, let H represent the finite difference counterpart of L on the Chebyshev staggered grid.

The eigenvalues of some channel flow cases are shown in Figure 2. There are no significant differences between these results and those for the model problem. The eigenvalue distribution for the boundary layer is slightly broader than for the channel. See Reference 14 for some boundary layer eigenvalues.

A useful alternative to the Chebyshev iterative method discussed in the preceding sub-section is a class of variational iterative methods.[18] The

simplest such scheme is called the minimum residual (MR) method. The preconditioned version begins with an initial guess X_o, the initial residual $R_o = B - LX_o$ and the initial direction Q_o, determined by $HQ_o = R_o$, and proceeds according to

$$\zeta_\ell = (R_\ell, LQ_\ell)/(LQ_\ell, LQ_\ell)$$

$$X_{\ell+1} = X_\ell + \zeta_\ell Q_\ell \tag{37}$$

$$R_{\ell+1} = R_\ell - \zeta_\ell LQ_\ell$$

$$HQ_{\ell+1} = R_{\ell+1} \ .$$

Like the Richardson scheme, this method requires one evaluation of the spectral operator (for LQ_n) and one solution of the implicit finite-difference system (for Q_{n+1}) per iteration. A sufficient condition for convergence is that the symmetric part of LH^{-1} be positive definite. The constant γ that appears in Equations (21) and (22) is used to ensure that this condition is met. (One can easily show that γ has no effect upon the eigenvalues of $H^{-1}L$, but that it does influence the symmetric part of LH^{-1}.)

Let us return momentarily to the model problem. For $\gamma = 1$, the extreme eigenvalues of the symmetric part of LH^{-1} are 1.59 and 0.71 for the case shown in Figure 1(a) whereas they are 18.8 and -15.6 for Figure 1(b). The MR method will clearly fail for the latter case. However, for $\gamma = 1/\sqrt{\hat{k}_x^2 + \hat{k}_z^2}$ these latter eigenvalues improve to 2.55 and 0.43. The importance of γ is evident. It is even more important when there is appreciable diffusion. The γ=1 extreme eigenvalues are 474 and -471 for Figure 1(f). The choice

$$\gamma = \left[1 + dk_{max}^2\right] / \sqrt{\hat{k}_x^2 + \hat{k}_z^2 + k_{max}^2} \ ,$$

where $k_{max} = N_y/2$ leads to 2.98 and 0.98. This scaling is based on balancing the norms of the diffusion and gradient operators. The principle applies to the actual channel and boundary layer problems as well.

There is clearly the prospect of future improvements in the preconditioning and scaling. One intriguing scheme is suggested by the observation that if a non-staggered grid were used for the pressure, then the preconditioning problems would shift from the averaging operator (which would become the identity) to the first derivative operator. Perhaps one should employ a scheme which alternates iterations on a staggered grid with ones on a non-staggered grid.

The preconditioning matrix H is block-tridiagonal. Note that Equation (27) can be separated into 2 independent real systems. Although we have no proof that the linear system $HQ_{n+1} = R_{n+1}$ from Equation (37) can be inverted without pivoting, we have yet to encounter a case which requires it for numerical stability, provided that the equations are ordered as suggested in Reference 14 and scaled as suggested above. We have, of course, made comparison with calculations performed with and without pivoting. We have also made several production runs in both 32-bit and 64-bit arithmetic and found 5 digit agreement. Furthermore, substantial round-off errors arising during the solution of the linear equations should prevent the iterative scheme from converging and this has not been observed. (The MR method, when convergent, has the property that the residual can be reduced to an arbitrarily small level, regardless of the precision of the machine.)

Time Discretization

This algorithm does not resort to splitting.[1] Although a splitting scheme would permit a simpler iterative method, this approach appears inadvisable for a general code in view of the demonstration by Marcus[21] for Taylor-Couette flow that the standard splitting scheme produces errors that do not vanish as Δt tends to zero.

The Crank-Nicolson treatment of the mean vertical diffusion term is standard and is essential for practical calculations at low Reynolds number. If needed, a semi-implicit treatment of horizontal diffusion can be readily incorporated into the algorithm. Moreover, the mean streamwise advection may also be treated semi-implicitly.

A backwards Euler treatment of the pressure appears to be all that is warranted. This variable merely serves as a constraint for enforcing the incompressibility condition. The pressure term has the character of an advection term with an infinite speed. The potential hazards of Crank-Nicolson for advection terms are well-known. We ourselves have encountered some difficulty with the use of Crank-Nicolson on the pressure in problems characterized by rapid decay of the interesting components of the solution. One such case is the Stokes layer in channel flow with one oscillating wall. The computed velocity decays properly but the pressure does not. It quickly attains an amplitude which does not vary with time and it changes sign every time step. No such difficulty arises when the backward Euler scheme is used for the pressure. Moreover, the velocity agrees with that of the former calculation. We have made numerous comparisons of the two pressure treatments in more conventional problems in which the solution grows or only slowly decays. In no case has there been any detectable difference in the

velocities. Evidently, the overall time accuracy of the algorithm is not degraded by the backward Euler pressure scheme.

Many transition and turbulence simulations have used second-order Adams-Bashforth (AB2) for the advection term. Both this method and explicit second-order Runge-Kutta (RK2) methods for a Fourier spatial discretization of advection suffer from weak instability. For a given spatial grid the fully discrete equations have a parasitic solution with a positive growth rate which is proportional to Δt (in terms of the physical time). This means that the computed solution is destined to blow up if integrated long enough. The useable time interval can be increased by reducing Δt, but this can be burdensome for long time integrations.

Higher-order time-stepping methods have the advantage of asymptotic stability as well as improved accuracy. A practical advection stability condition has the form

$$\Delta t \leq c \left[\frac{\Delta x}{u_{max}} + \pi \left(\frac{\Delta y}{v} \right)_{max} + \frac{\Delta z}{w_{max}} \right] \tag{38}$$

where c is a CFL parameter. The formal limits on c are 0.23 for AB3, 0.13 for AB4, 0.55 for RK3, and 1.27 for RK4. In terms of execution time for a calculation operated at the stability limit, AB3 is favored over RK3 and RK4 over AB4.

The Navier-Stokes algorithm with a conventional third-order advection scheme requires storage for 10 variables. (The pressure is needed only at the latest time level.) Williamson[22] has catalogued numerous low storage Runge-Kutta schemes that, when modified to the present application with its additional implicit terms, require storage for only 7 variables. For the equation

$$u_t = F + G,$$

where the terms in F are treated by RK3 and those in G by Crank-Nicolson, such a scheme reads

$$\begin{aligned}
H_1 &= \Delta t F_o \\
u_1 &= u_o + \frac{1}{3} H_1 + \frac{1}{6} \Delta t(G_o + G_1) \\
H_2 &= \Delta t F_1 - \frac{5}{9} H_1 \\
u_2 &= u_1 + \frac{15}{16} H_2 + \frac{5}{24} \Delta t(G_1 + G_2) \\
H_3 &= \Delta t F_2 - \frac{153}{128} H_2 \\
u_3 &= u_2 + \frac{8}{15} H_3 + \frac{1}{8} \Delta t(G_2 + G_3)
\end{aligned} \tag{39}$$

where $u_o = u^n$ and $u_3 = u^{n+1}$. The inclusion of G makes this scheme formally second-order accurate for advection. However, in our own calculations for low viscosity flows we have found it to have errors at most 50% greater than those for a true third-order advection scheme. Moreover, the errors decrease by a factor of 8 when Δt is halved, even down to an accuracy level of 6 significant digits. The scheme (39) is to be preferred when storage is at a premium or the I/O costs are substantial.

Implementation

Both the channel and boundary-layer versions of this algorithm have been implemented on a Control Data Corporation Cyber 175. The channel code has recently been made operational on the Control Data Corporation VPS 32 (a vector processor which is architecturally similar to a two-pipe Cyber 205, but expanded to over 16 million 64-bit words of memory).

No special coding was used for the scalar Cyber 175 code, except for the assembly language FFT's. The code has been used for calculations on collocation grids as large as 16 x 32 x 8. A typical channel application requires 3 msec per time step per grid point for a convergence criterion on the iterative scheme sufficient to ensure that the velocity field is divergence free to better than 1 part in 10^{10}. (If the 2/3 rule is used to de-alias the horizontal directions, then this time is reduced substantially--roughly by half--since most of the CPU time is spent in solving the implicit equations.) The run time does depend on the amplitude of the disturbances. It varies by perhaps a factor of 2 in either direction from the figure cited above. The boundary-layer code, with fixed temperature, takes perhaps 20% more time per step.

The VPS 32 code has been implemented entirely in Cyber 200 Fortran. The FFT's were written by the authors using the guidelines given by Temperton.[23] They currently incorporate radix 2 and radix 3. Vectorization of the implicit equation solution was achieved by solving for many pairs $(\hat{k}_x, \hat{k}_z)$ simultaneously with no pivoting. Typically 1/4 of all the pairs were solved for at a time. On a 32^3 grid the vector lengths for the block-tridiagonal inversions and for many parts of the residual calculation are only 136. The VPS 32 requires somewhat longer vectors to operate near its peak capacity.

For a 64^3 grid, however, the vector length is over 500, which is much more acceptable. A typical calculation on a 32^3 grid requires 2.5 sec per step, whereas the corresponding 64^3 calculations take 10 sec per step. This increase in time by a factor of 4 rather than 8 is indicative of the improved performance of the VPS 32 as the vector length increases. (With aliasing control these times are halved.)

We have also implemented a version of this code which uses finite differences in the normal direction. It takes 0.5 sec per step on a 32^3 grid and 3 sec per step on a 64^3 grid. These calculations proceed at a sustained speed of over 90 MFLOPS in 64-bit arithmetic. Clearly, the CPU time penalty for spectral resolution in the normal direction is not unduly severe.

APPLICATIONS

Channel Flow

The usual scaling for the channel is employed. Lengths are scaled by channel half-width and velocities by the centerline velocity of the mean flow. A uniform density of unity is presumed. The Reynolds number is based on channel half-width and the mean centerline velocity.

Parallel shear flows admit one set of linear waves which are solutions to the Orr-Sommerfeld equation and another set which are solutions to the unforced Squire equation. The linear waves for the channel can be further delineated into wall modes and center modes. The former have phase speeds of roughly 0.3, and their most significant details are located near the walls. The Orr-Sommerfeld wall modes are, of course, the familiar Tollmein-Schlichting (TS) waves. Although the Squire wall modes (SW) are themselves

linearly stable, weakly nonlinear theories have indicated that they may interact with TS waves, even some linearly stable ones, in such a way as to trigger instability. The center modes, both the Orr-Sommerfeld ones (OSC) and the Squires ones (SC), have phase speeds roughly 0.9, and their energy is concentrated near the center of the channel.

Because of the availability of experimental[6] and computational[7] results, an obvious test case is Re = 5000. Table I summarizes the properties of several linear modes. Columns 4 and 5 list the real and imaginary parts of the temporal eigenvalues ω, as determined by the numerical solution of the linear eigenvalue problem. The last column in Table I lists the growth rates estimated from numerical simulations using as initial conditions just the mean flow plus a linear mode at 0.001% amplitude, where the eigenfunctions are normalized so that they have a maximum streamwise velocity component of 1. The calculated growth rates were obtained from a least squares fit to the perturbation kinetic energy over the time interval [0,50]. These particular calculations used $N_y = 48$ and the AB3 scheme with $\Delta t = 0.100$. This seems to be adequate evidence for the consistency of the present semi-implicit, unsplit, collocation, staggered grid spectral algorithm.

The time history of the kinetic energy in selected harmonics is displayed in Figure 3 for a more interesting calculation. This Re = 5000 run on a $16 \times 32 \times 16$ grid began with the two-dimensional TS wave of Table I at 5% amplitude and the usual Benney-Lin combination of two oblique TS waves at a combined amplitude of 0.1%. The lowest harmonics retained in the calculations were 1.12 in x and 2.00 in z. The time step was $\Delta t = 0.05$. The individual harmonics are labeled by integers which denote the wavenumbers relative to those of the three-dimensional TS waves. The modal energies are measured

relative to the energy in the mean flow and include contributions from symmetrical components; e.g., the (1,-1), (-1,1), and (-1,-1) components are included in the harmonic labelled (1,1). Nonlinear effects produce the familiar secondary instability which is indicated by the growth of the (1,1) mode.

Heated, Parallel Boundary Layer

The controlled, incompressible boundary layer has not yet been explored by three-dimensional numerical simulation. The principal LFC techniques can be incorporated into the parallel boundary layer approximation as described in the second section. We report here some of the tests of the present algorithm which were performed with the low resolution Cyber 175 code with temporally frozen temperature.

The case* Re = 8950 has been singled out in the past for investigations based on linear theory.[11] The strongest instability occurs for $\alpha = 0.158266$, $\beta = 0$ and has a complex frequency $\omega = 0.036797 + i\ 0.003550$. Each of the principal LFC techniques can completely stabilize flow at this Reynolds number, at least linearly. Table II lists the amount of control required to reduce the growth rate of the strongest instability to roughly 0.0001. This table includes the wavenumbers and frequencies of the least stable (two-dimensional) waves, as well as the frequency of the three-dimensional wave with $\beta = \alpha$. The last column is indicative of the accuracy of the numerical simulations. It lists the growth rates estimated by a least squares fit to

*Bushnell, D. M., M. Y. Hussaini, and T. A. Zang, "Sensitivity of LFC Techniques in the Nonlinear Regime," to appear.

the perturbation kinetic energy for a calculation starting with an initial TS wave of 0.01% amplitude and lasting until $t = 500$. The time-step was $\Delta t = 1$ and the vertical resolution was $N_z = 40$. The integration time covers well over two periods of each wave. The discrepancy between the growth rates estimated from the simulation and those predicted by linear theory is of the same order as the accuracy of the latter.

Figure 4 demonstrates that the heated boundary layer is susceptible to the secondary instability. This calculation was performed on a $16 \times 32 \times 8$ grid with a time step $\Delta t = 0.5$. The usual initial three-dimensional Benney-Lin mode had an amplitude of 0.01% and the two-dimensional TS wave started at the 5% level. The time histories of the harmonic components are very similar to those for the secondary instability of the channel wall modes.

Numerous other examples for both the channel and the boundary layer may be found in reference 24.

CONCLUDING REMARKS

This paper has been devoted to a detailed description of a fully spectral algorithm that we are presently employing to investigate stability and transition in controlled, parallel boundary layers. This method is particularly well-suited to accounting for the subtle, time-dependent effects of heating and of temperature fluctuations upon the viscosity and conductivity.

This algorithm may be extended to other applications as well. It can, for example, be used for large-eddy simulations or for other simulations of turbulence which employ a spatially and temporally varying eddy viscosity. Moreover, it may also be applied to compressible flow problems.

REFERENCES

1. Orszag, S. A.; and Kells, L.C.: Transition to Turbulence in Plane Poiseuille and Plane Couette Flows. J. Fl. Mech., Vol. 96, January 1980, pp. 159-205.

2. Benney, D. J.; and Lin, C. C.: On the Secondary Motion Induced by Oscillation in a Shear Flow. Phys. Fluids, Vol. 3, No. 4, August 1960, p. 656.

3. Wray, A.; and Hussaini, M. Y.: Numerical Experiments in Boundary-Layer Stability. AIAA Paper No. 80-0275.

4. Kovasznay, L. S.; Komoda, H.; and Vasudeva, B. R.: Proc. 1962 Heat Transfer and Fluid Mechanics Institute, Stanford Univ. Press, 1962, pp. 1-26.

5. Orszag, S. A.; and Patera, A. T.: Secondary Instability of Wall-Bounded Shear Flows. J. Fl. Mech., Vol. 128, March 1983, pp. 347-385.

6. Nishioka, M.; Asai, M.; and Iida, S.: An Experimental Investigation of the Secondary Instability in Laminar-Turbulent Transition. R. Eppler, H. Fasel, eds., pp. 37-46, Springer, 1980.

7. Kleiser, L.; and Schumann, U.: Spectral Simulation of the Laminar-Turbulent Transition Process in Plane Poiseuille Flow. Proc. of ICASE Symposium on Spectral Methods, (R. Voigt, D. Gottlieb, and M. Y. Hussaini, eds.), SIAM-CBMS, 1984, pp. 141-163.

8. Moser, R. D.; Moin, P.; and Leonard, A.: A Spectral Numerical Method for the Navier-Stokes Equations with Applications to Taylor-Couette Flow. J. Comp. Phys., Vol. 52, No. 9, December 1983, pp. 524-544.

9. Morchoisne, Y.: Pseudo-Spectral Space-Time Calculations of Incompressible Viscous Flow. AIAA Paper 81-0109.

10. Schlichting, H.: Boundary Layer Theory, 7th Edition, McGraw-Hill, 1979.

11. Lowell, R. L.; and Reshotko, E.: Case Western Reserve University, FT AS/TR-73-93, 1974.

12. Malik, M. R.; Chuang, S.; and Hussaini, M. Y.: Accurate Numerical Solution of Compressible Stability Equations. ZAMP, Vol. 33, No. 2, March 1982, pp. 189-201.

13. Orszag, S. A.: Accurate Solution of the Orr-Sommerfeld Equation. J. Fl. Mech., Vol. 50, No. 4, December 1971, pp. 689-703.

14. Malik, M. R.; Zang, T. A.; and Hussaini, M. Y.: A Spectral Collocation Method for the Navier-Stokes Equations. J. Comp. Phys., to appear.

15. Brachet, M. E., et al.: Small-Scale Structure of the Taylor-Green Vortex. J. Fl. Mech., Vol. 130, May 1983, pp. 411-452.

16. Orszag, S. A.: Spectral Methods for Problems in Complex Geometries. J. Comp. Phys., Vol. 37, No. 2, August 1980, pp. 70-92.

17. Hageman, L. A. and Young, D. M.: Applied Iterative Methods, Academic Press, 1981.

18. Eisenstat, S. C.; Elman, H. C.; and Schultz, M. H.: Variational Iterative Methods for Nonsymmetric Systems of Linear Equations. SIAM J. Numer. Anal., Vol. 20, No. 2, April 1983, pp. 345-357.

19. Zang, T. A.; Wong, Y-S; and Hussaini, M. Y.: Spectral Multigrid Methods for Elliptic Equations II. J. Comp. Phys., Vol. 54, No. 3, June 1984, pp. 489-507.

20. Manteuffel, T. A.: The Tchebyshev Iteration for Nonsymmetric Linear Systems. Numer. Math., Vol. 28, No. 3, 1977, pp. 307-327.

21. Marcus, P.: Simulation of Taylor-Couette Flow--Numerical Methods and Comparison with Experiment. J. Fl. Mech., to appear.

22. Williamson, J. H.: Low-Storage Runge-Kutta Schemes. J. Comp. Phys., Vol. 35, No. 1, March 1980, pp. 48-56.

23. Temperton, C.: Self-Sorting Mixed-Radix Fast Fourier Transforms. J. Comp. Phys., Vol. 52, No. 1, October 1983, pp. 1-23.

24. Zang, T. A. and Hussaini, M. Y.: Numerical Experiments on Subcritical Transition Mechanisms, AIAA Paper No. 85-0296.

Table I. Some Channel Modes for Re = 5000

Mode	α	β	ω_r	ω_i	$\omega_{i\|calc}$
TS 2-D	1.12	0.00	0.315563	-0.002783	-0.002783
TS 3-D	1.12	2.00	0.364473	-0.076227	-0.076234
SW 3-D	0.56	2.00	0.125129	-0.069908	-0.069889
OSC 2-D	1.12	0.00	1.067058	-0.052467	-0.052466
OSC 3-D	1.12	2.00	1.066915	-0.051005	-0.050997

Table II. Some Controlled Boundary-Layer Modes for Re = 8950

Control	Mode	α	β	ω_r	ω_i	$\omega_{i\|calc}$
$\beta_p = 0.55$	TS 2-D	0.167675	0.00	0.037384	0.000095	0.000096
	TS 3-D	0.167675	0.167675	0.040948	-0.001012	-0.001028
$F_W = 0.895$	TS 2-D	0.162057	0.00	0.036207	0.000093	0.000093
	TS 3-D	0.162057	0.162057	0.039742	-0.000968	-0.000993
$\tau = 1.10$	TS 2-D	0.149937	0.00	0.029337	0.000093	0.000097
	TS 3-D	0.149937	0.149937	0.032106	-0.000798	-0.000793

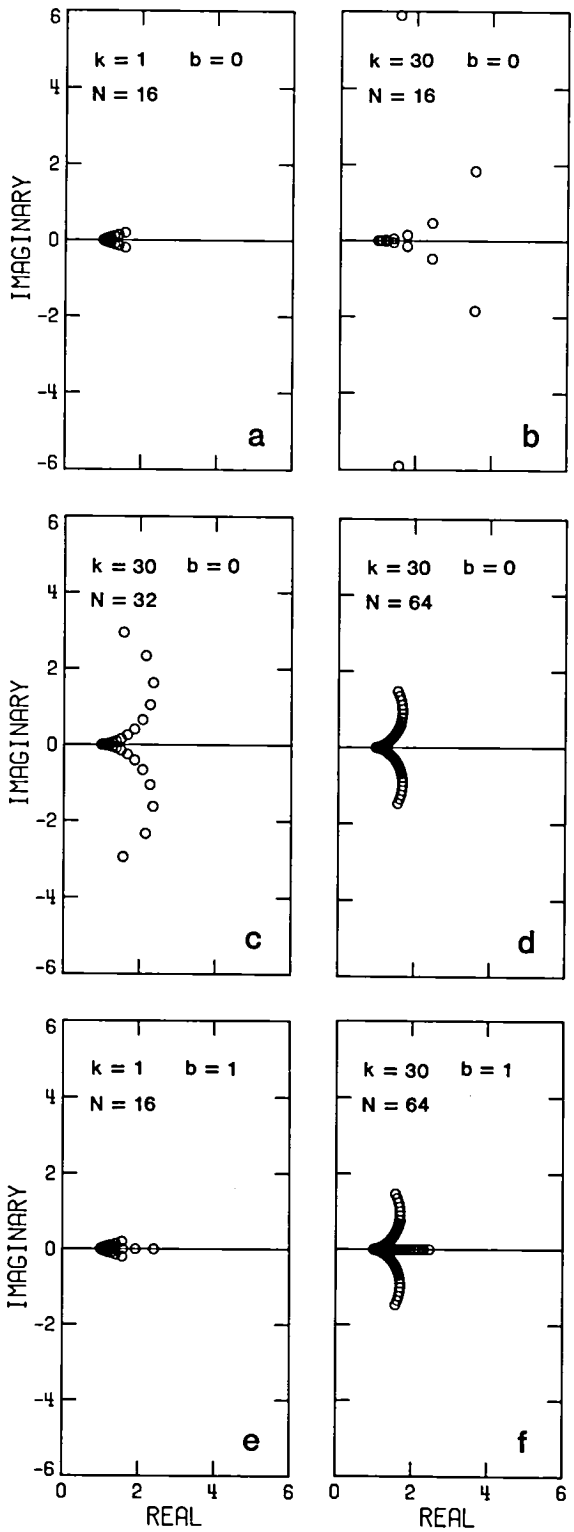

Figure 1. Eigenvalues of $\hat{H}^{-1} L$ for the model problem. Here k denotes the value of k_x and $k_z = 0$.

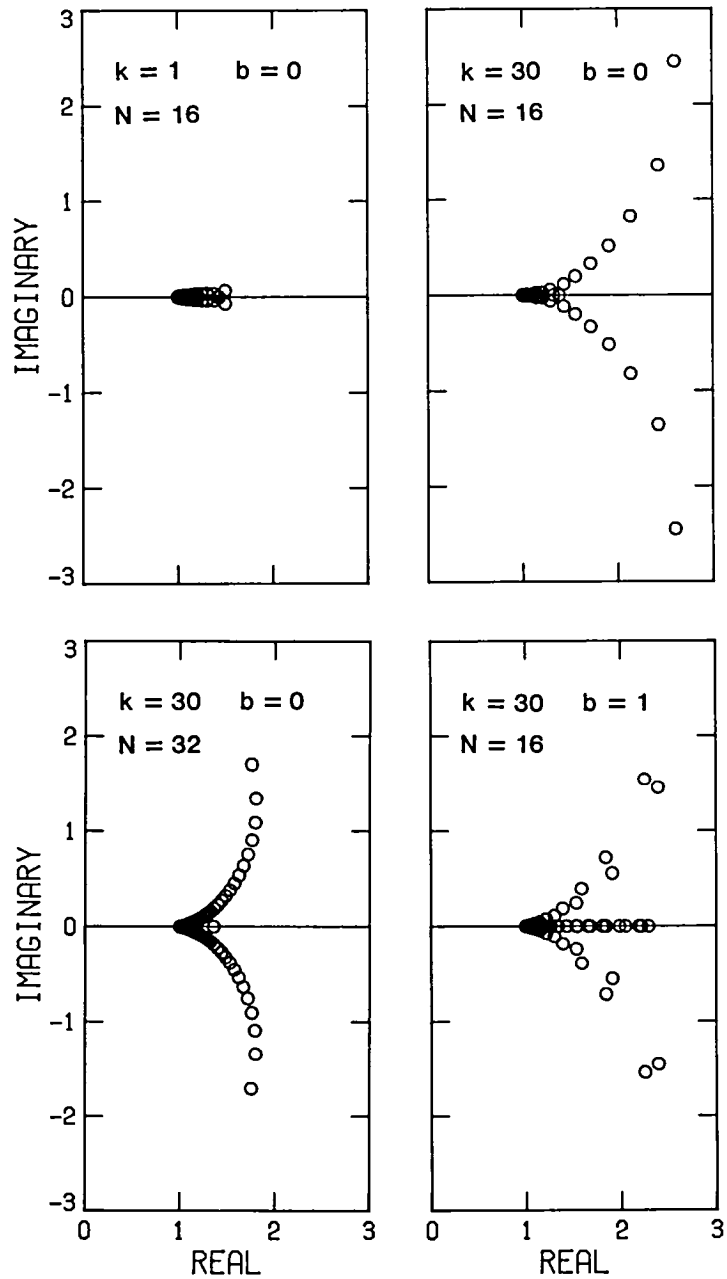

Figure 2. Eigenvalues of $\hat{H}^{-1}\hat{L}$ for channel flow. Here k denotes the values of k_x and k_z.

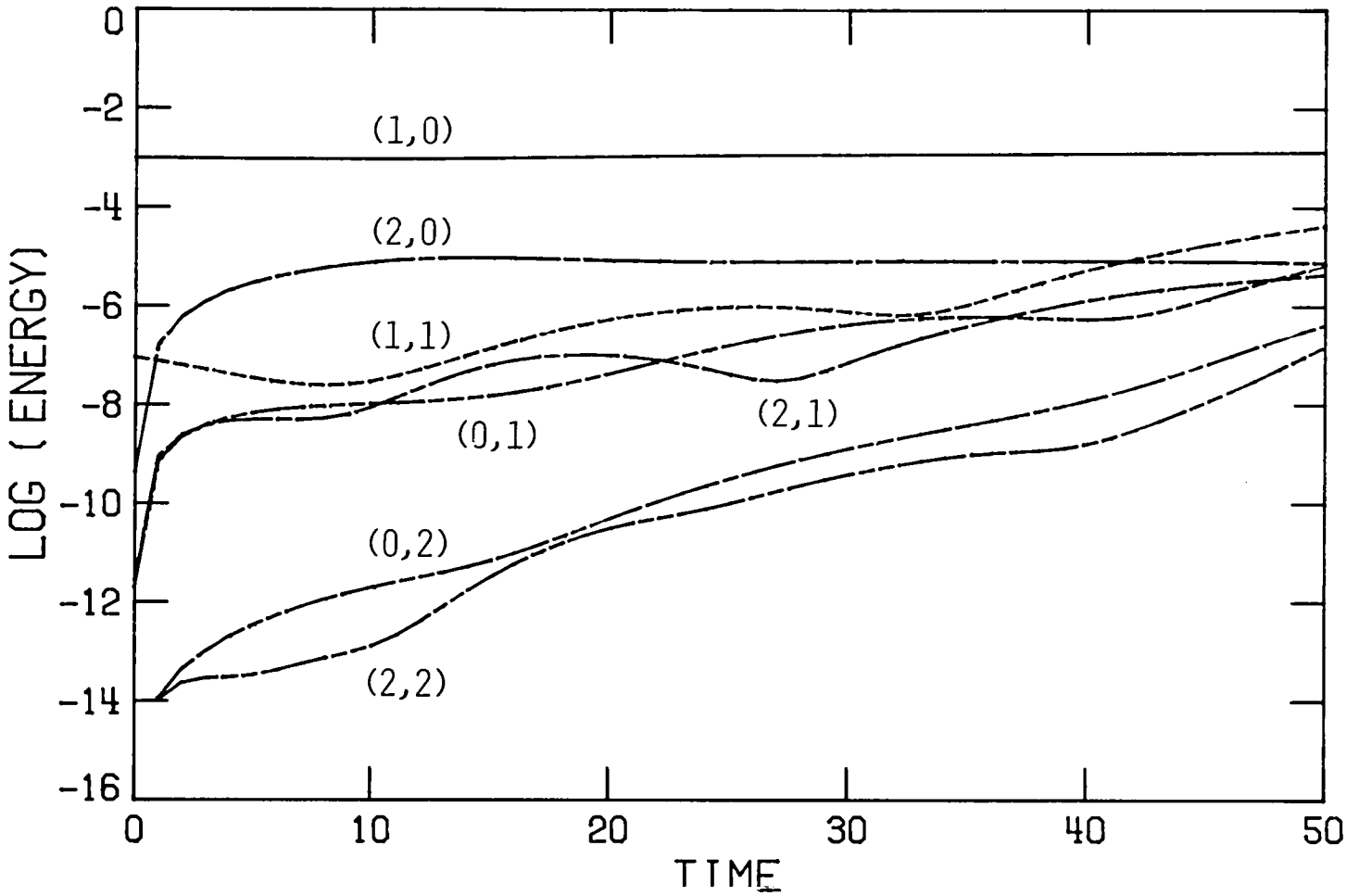

Figure 3. Harmonic history for a Re = 5000 channel flow simulation starting with a 5% two-dimensional TS wave and a 0.1% combination of 2 three-dimensional TS waves. The harmonics are labelled by their respective streamwise and spanwise wavenumbers relative to those of the three-dimensional TS wave with $\alpha = 1.12$ and $\beta = 2.00$.

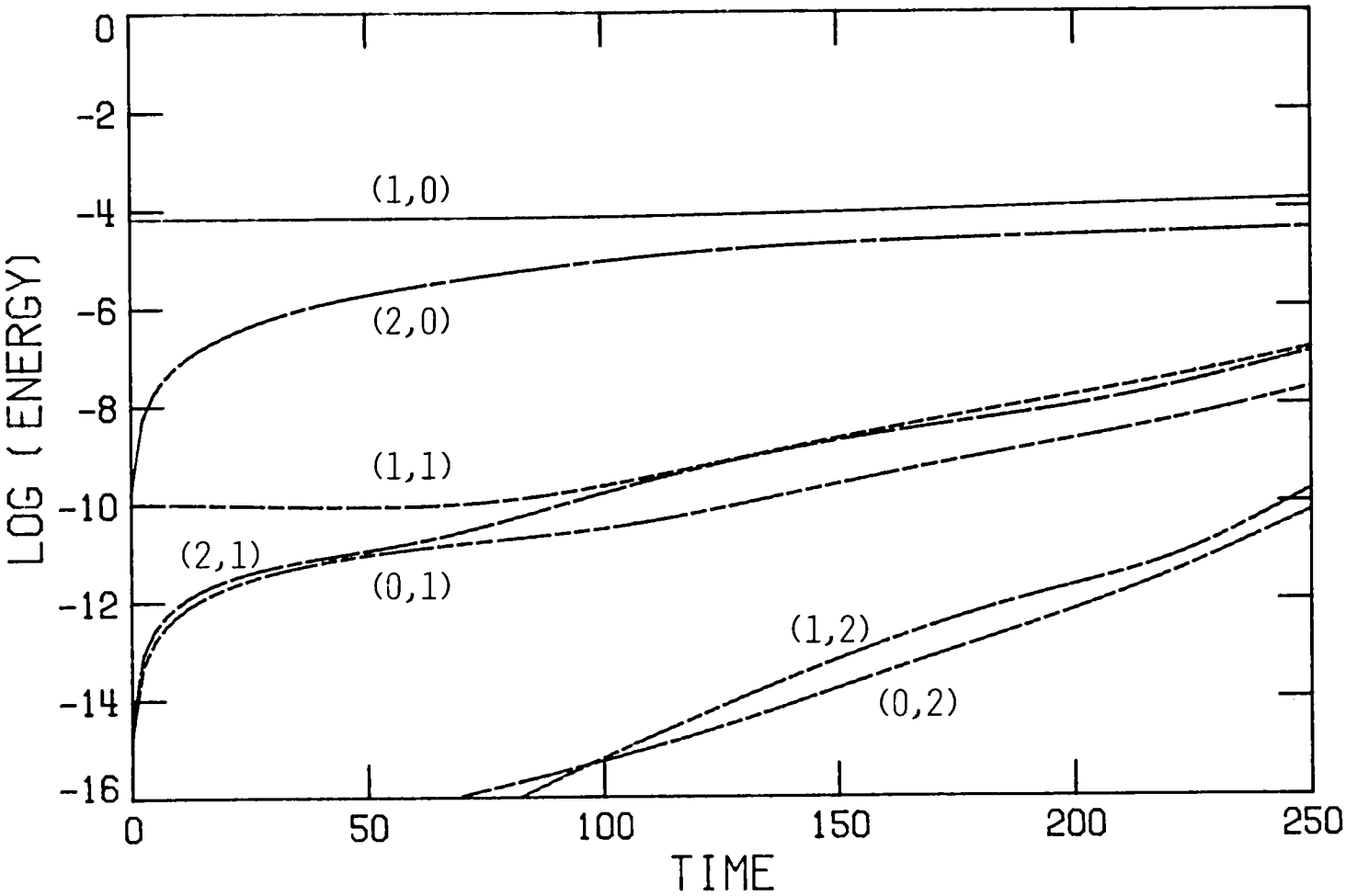

Figure 4. Harmonic history for a Re = 8950 heated boundary layer simulation starting with a 5% two-dimensional TS wave and a 0.01% combination of 2 three-dimensional TS waves. The harmonics are labelled by their respective streamwise and spanwise wavenumbers relative to those of the three-dimensional TS wave with $\alpha = 0.150$ and $\beta = 0.150$.

1. Report No. NASA CR-172561 ICASE Report No. 85-19	2. Government Accession No.	3. Recipient's Catalog No.
4. Title and Subtitle A THREE-DIMENSIONAL SPECTRAL ALGORITHM FOR SIMULATIONS OF TRANSITION AND TURBULENCE		5. Report Date March 1985 6. Performing Organization Code
7. Author(s) Thomas A. Zang and M. Yousuff Hussaini		8. Performing Organization Report No. 85-19 10. Work Unit No.
9. Performing Organization Name and Address Institute for Computer Applications in Science and Engineering Mail Stop 132C, NASA Langley Research Center Hampton, VA 23665		11. Contract or Grant No. NAS1-17070 13. Type of Report and Period Covered Contractor Report
12. Sponsoring Agency Name and Address National Aeronautics and Space Administration Washington, D.C. 20546		14. Sponsoring Agency Code 505-31-83-01

15. Supplementary Notes

Langley Technical Monitor: J. C. South, Jr.
Final Report
Presented at the AIAA 23rd Aerospace Sciences Meeting, January 14-17, 1985, Reno, NV

16. Abstract

A spectral algorithm for simulating three-dimensional, incompressible, parallel shear flows is described. It applies to the channel, to the parallel boundary layer, and to other shear flows with one wall-bounded and two periodic directions. Representative applications to the channel and to the heated boundary layer are presented.

17. Key Words (Suggested by Author(s))	18. Distribution Statement
spectral methods transition laminar flow control	34 - Fluid Mechanics & Heat Transfer Unclassified - Unlimited

19. Security Classif. (of this report)	20. Security Classif. (of this page)	21. No. of Pages	22. Price
Unclassified	Unclassified	40	A03

For sale by the National Technical Information Service, Springfield, Virginia 22161

NASA-Langley, 1985